Journal of Geodynamics 89 (2015) 29–38

Contents lists available at ScienceDirect

Journal of Geodynamics

journal homepage: http://www.elsevier.com/locate/jog

Deformation structures in the frontal prism near the Japan Trench: Insights from sandbox models

Santanu Bose[a,*], Puspendu Saha[a], James J. Mori[b], Christie Rowe[c], Kohtaro Ujiie[d], Frederick M. Chester[e], Marianne Conin[f], Christine Regalla[c], Jun Kameda[g], Virginia Toy[h], James Kirkpatrick[c], Francesca Remitti[i], J. Casey Moore[j], Monica Wolfson-Schwehr[k], Yasuyuki Nakamura[l], Anchit Gupta[m]

[a] Department of Geology, Experimental Tectonic Laboratory, University of Calcutta, 35 Ballygunge Circular Road, Kolkata 700 019, India
[b] Disaster Prevention Research Institute, Kyoto University Gokasho, Uji Kyoto 611-0011, Japan
[c] Earth and Planetary Sciences Department, McGill University, 3450 University Street, Montreal, QC H3A 0E8, Canada
[d] Graduate School of Life and Environmental Sciences, University of Tsukuba, 1-1-1 Tennodai, Tsukuba 305-0006, Japan
[e] Center for Tectonophysics, Department of Geology and Geophysics, Texas A&M University, College Station, TX 77843-3115, USA
[f] Universite de Lorraine, CNRS, CREGU, GeoRessources laboratory, Nancy School of Mines, Nancy F-54000, France
[g] Earth and Planetary Sciences, Faculty of Science, Hokkaido University, Sapporo 060-0810, Japan
[h] Department of Geology, University of Otago, 360 Leith Walk, Dunedin 9054, New Zealand
[i] Dipartimento di Scienzedella Terra, Università di Modena e Reggio Emilia largo, S. Eufemia, 19, 41100 Modena, Italy
[j] Department of Earth and Planetary Sciences, University of California Santa Cruz, 1156 High, St., Santa Cruz, CA 95064, USA
[k] Center for Coastal and Ocean Mapping, Joint Hydrographic Center, University of New Hampshire, 24 Colovos Road, Durham, NH 03824, USA
[l] Institute for Research on Earth Evolution, JAMSTEC, Yokohama, Japan
[m] Department of Earth Sciences, Indian Institute of Technology, Roorkee 247667, Uttarakhand, India

ARTICLE INFO

Article history:
Received 24 December 2014
Received in revised form 3 June 2015
Accepted 9 June 2015
Available online 11 June 2015

Keywords:
Sandbox experiments
Inner and outer wedge
Slope-break
Horst-and-graben structure
Fault friction

ABSTRACT

We have used sandbox experiments to explore the mechanics of the frontal prism structures documented by seismic reflection data and new borehole from IODP Expedition 343 (JFAST). This study investigated the effects of down-dip (normal to trench axis) variations in frictional resistance along a decollement on the structural development of the frontal wedges near subduction zones. Interpretation of seismic reflection images indicates that the wedge has been effected by trench-parallel horst-and-graben structures in the subducting plate. We performed sandbox experiments with down-dip patches of relatively high and low friction on the basal decollement to simulate the effect of variable coupling over subducting oceanic plate topography. Our experiments verify that high frictional resistance on the basal fault can produce the internal deformation and fault-and-fold structures observed in the frontal wedge by the JFAST expedition. Subduction of patches of varying friction caused a temporal change in the style of internal deformation within the wedge and gave rise to two distinctive structural domains, separated by a break in the surface slope of the wedge: (i) complexly deformed inner wedge with steep surface slope and (ii) shallow taper outer wedge, with a sequence of imbricate thrusts. Our experiments further demonstrate that the topographic slope-break in the wedge develops when the hinterland part of the wedge essentially stops deforming internally, leading to in-sequence thrusting with the formation of an outer wedge with low taper angle. For a series of alternate high and low frictional conditions on the basal fault the slope of the wedge varies temporally between a topographic slope-break and uniformly sloping wedge.

1. Introduction

It is now well known that the subduction of bathymetric features in the oceanic plate, e.g., seamounts, aseismic ridges, volcanic plateaux has a strong influence on the development of morphological features and deformation structures in the overriding plate

* Corresponding author. Tel.: +91 9433501266.
E-mail address: bose.santanu@gmail.com (S. Bose).

http://dx.doi.org/10.1016/j.jog.2015.06.002
0264-3707/

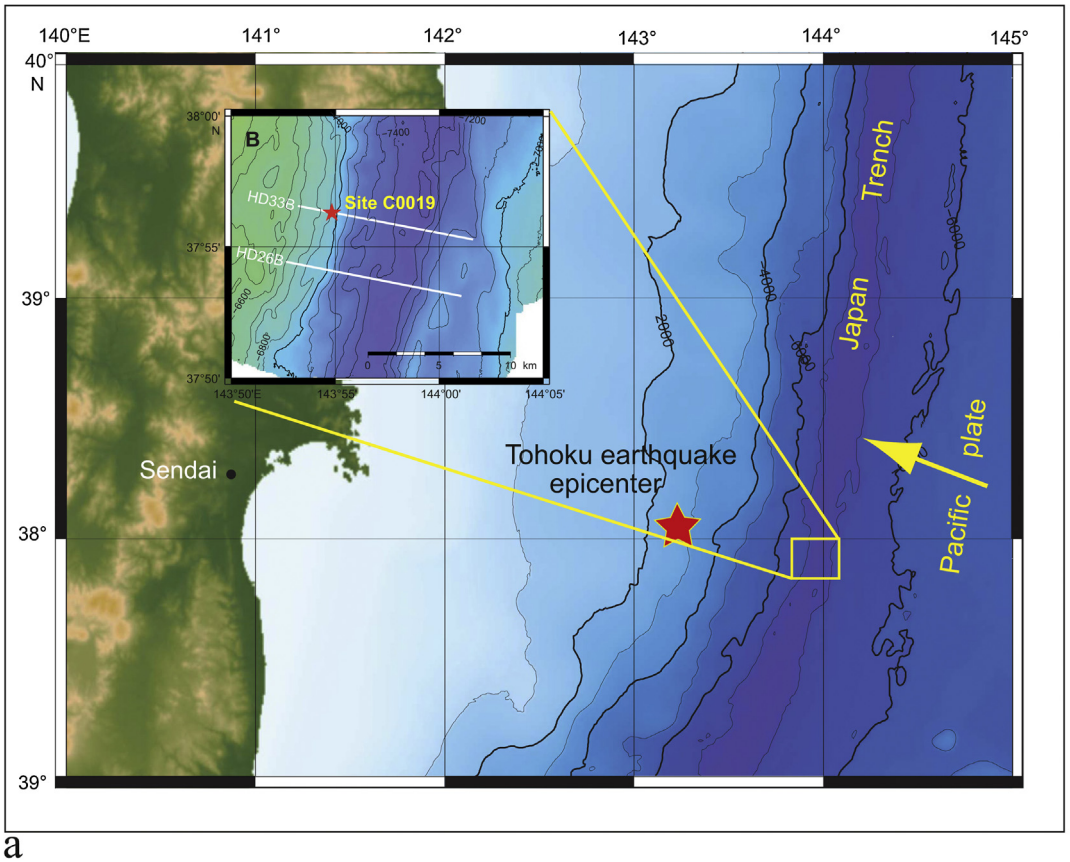

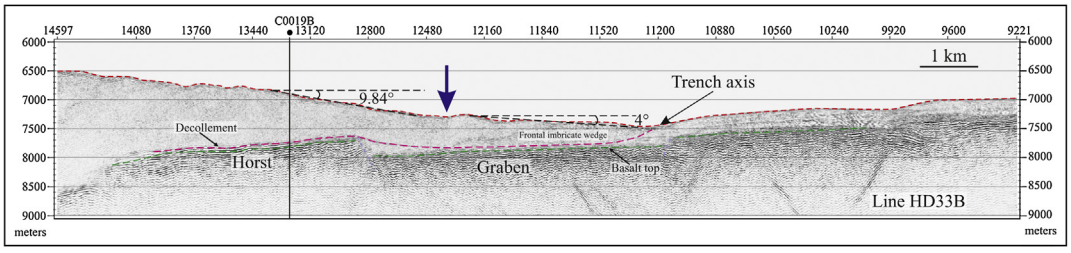

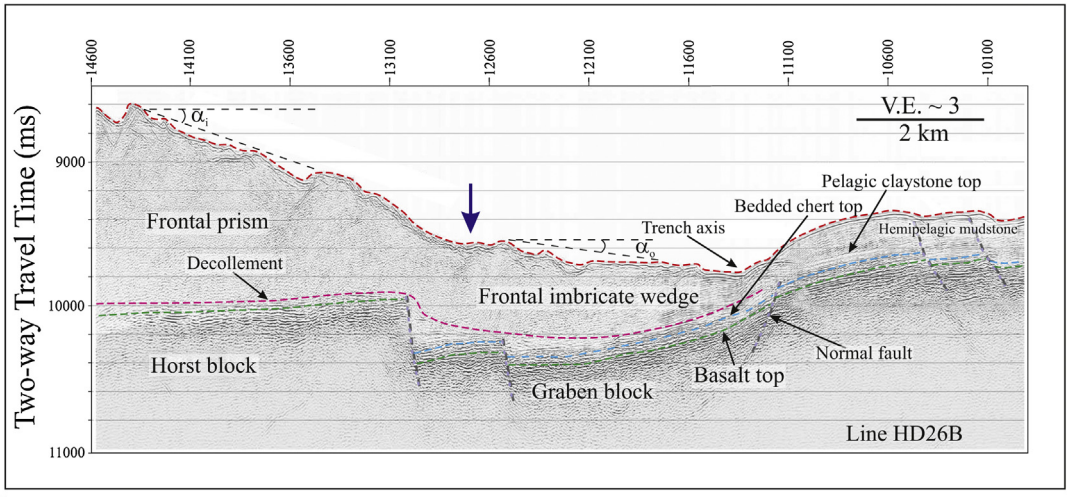

Fig. 1. (a) Location map, showing the eastern coastline of Honshu, bathymetry near Japan Trench and Tohoku earthquake epicenter (red star). The yellow arrow indicates the direction of plate convergence. Inset map shows location of Expedition 343 site C0019 (red star) along seismic section Line HD 33B (Fig. 1b). Line HD 26B another seismic section line shown in Fig. 1c. (b) Image of seismic section Line HD 33B crossing the IODP drilling site C0019 with no vertical exaggeration. It shows change in topographic slope (marked red lines) from inner wedge (~10°) to outer wedge (~4°) (modified after Nakamura et al., 2013). (c) Image of seismic section Line 26B with V.E. ~3, separated

(Dominguez et al., 2000; Malavieille, 1984; von Huene and Culotta, 1989; von Huene and Lallemand, 1990; Lallemand et al., 1992, 1994; von Huene et al., 2004; Park et al., 1999; Wang and Hu, 2006). These studies indicate that the styles of deformation in the overriding plate vary with the geometry of bathymetric features in the subducting plate. For example, the subduction of seamounts correlates to a steeper surface slopes in the inner wedge than that in the outer wedge (Park et al., 1999; Dominguez et al., 2000). Conversely, the subduction of aseismic ridges causes the development of a steep outer wedge slope and with almost flat inner wedge (Lallemand et al., 1992). Despite dominance of horst-and-graben structure at many trenches, its influence on frontal wedge growth remains relatively unexplored. We therefore analyze the impacts of subducting horst-and-graben structures on the evolution of the frontal wedge near the Japan Trench.

Geophysical investigations along several sections across the Japan Trench (Fig. 1b and c) recorded a series of horst-and-graben structures on the subducting plate beneath the frontal wedge (Tsuru et al., 2002; Kodaira et al., 2012; Nakamura et al., 2013). Moreover, earlier studies have shown that the sediment thickness in the incoming Pacific plate near the Japan Trench is thin, and that the thinning of sediment thickness mostly occurs above the horst blocks (Groshong, 2006), potentially changing the surface roughness. The combination of the effects of the differences in sediment thickness and surface roughness over a horst-and-graben structure in the subducting plate causes varying degrees of coupling at the plate interface, creating varying frictional properties on the decollement (Pacheco et al., 1993; Tanioka et al., 1997; von Huene et al., 1999; Bilek, 2007; Das and Watts, 2009). In the present study we have used sandbox experiments to simulate the effects of down-dip variations in the frictional strength on the decollement to investigate the structural development of frontal wedge and finally, provide a mechanical model for explaining the structural evolution of the frontal wedge over subducting horsts and grabens at the Japan Trench.

Integrated Ocean Drilling Program (IODP) Expedition 343 (JFAST) drilled to a depth of 836 m below seafloor (mbsf) near the Japan Trench at site C0019, penetrating the plate boundary decollement above a subducting horst, located about ~7 km westward from the trench axis (Fig. 1a). Seismic reflection images collected before and after the drilling expedition have been interpreted to understand the tectonic evolution of the frontal wedge (Nakamura et al., 2013). Geophysical logs and core samples collected during the expedition have provided a great opportunity to compare our experimental results with observed deformation structures within the frontal wedge (Chester et al., 2013; Kirkpatrick et al., 2014).

2. Experimental methods and materials

Sandbox experiments have proved to be useful in understanding the mechanics of thin-skinned accretionary wedges using the concept of critical taper theory (Chapple, 1978; Boyer and Elliot, 1982; Davis et al., 1983; Dahlen, 1990). The angle of the critical taper is defined by the summation of the basal inclination (β) and surface slope (α). According to the critical taper model, a wedge deforms internally and thereby, increases its taper. At a critical taper angle ($\alpha+\beta$), the internal stress in the wedge equals the material's yield strength causing internal deformation, leading the wedge on the verge of failure. At this stage, the increase in shear stress on the base can drive frictional sliding at the decollement, maintaining the wedge at constant taper angle (Davis et al., 1983; Boyer and Elliot, 1982). It has been shown theoretically and experimentally that the angle of critical taper is proportional to the frictional condition on the basal decollement according to the following equation (Dahlen, 1990):

$$\alpha+\beta=(\beta+\mu_b)\left(\frac{1-\sin\phi_c}{1+\sin\phi_c}\right) \quad (1)$$

where, μ_b is the coefficient of static friction on the decollement and ϕ_c is the angle of internal friction of the frontal prism material.

In the present study, we have prepared our experimental models with varying down-dip frictional conditions on the decollement to simulate the effect of horst-and-graben structure along the basal decollement (Fig. 2). We have assumed that the horst behaves as an asperity characterized by enhanced coupling with the overriding plate, and modeled this by imparting a relatively higher frictional coefficient on the decollement to simulate a horst block. Thus the horst and graben structure gives rise to alternate zones of relatively strong and a weak contact respectively with the overriding plate on the decollement. In the laboratory scaled experiments the higher basal friction (μ_b = 0.46), simulating the decollement immediately above the horst block, was achieved by pasting commercial sand paper (P30, average grit size 622.0 μ) on a glass plate. A relatively lower basal friction (μ_b = 0.36) was obtained by sieving a veneer of boric acid powder (0.001 mm beads) over the glass plate in order to model the frictional strength above the graben sediments. However, in some experiments we pasted rigid block of 5 mm thick acrylic sheet over the basal glass plate to model the horst block. In this set of experiments, we had to stop the experiment once the buttress reached the edge of the acrylic block. Experimental results from these two different sets of experiments, however, show that frontal wedge propagation ceases once the decollement propagation reaches the high frictional patch/edge of the rigid acrylic sheet (see electronic supplementary Fig. S1). This finding suggests that the use of high frictional patch on the basal glass plate is a suitable analog for simulating natural horst-block configuration. The advantage of using sandpaper over rigid block is that the hinterland buttress can override the high frictional patch without limiting the amount of shortening during the experimental run.

In the model setup, Zone I represents a graben, simulating low frictional stress in the seismogenic plate interface and Zone II corresponds to a horst block with high frictional resistance in the subducting plate (Fig. 2). Although a majority of our experiments were carried out with one high frictional patch between zones of relatively lower friction on the basal fault, a few experiments were carried out with two zones of high frictional patches to understand the effects of a series of horst-and-graben structures. Experimental models were prepared by sieving sand layers from a constant height of 20 cm in a rectangular glass-walled sandbox apparatus over a rigid base of varying basal friction (μ_b) (Fig. 2). The length and width of the apparatus are 110 cm and 35 cm respectively. The model width was more than fifteen times its thickness to avoid the effects of friction at the interface of sand layers and the glass sidewalls (Souloumiac et al., 2012). The coefficients of basal friction (μ_b) were calculated separately from sliding experiments using dry non-cohesive sand. Note that the values of μ_b used in our experiments are merely represented qualitatively and do not correspond to the natural materials in the Japan Trench subduction thrust. The glass walls of the sandbox were cleaned and dried carefully to remove surface moisture. This process is important in order to prevent sticking of sand to the glass walls.

by 3.5 km from seismic line HD 33B. α_i and α_o are relative slopes of inner and outer wedges respectively, showing changes in topographic slope (modified after Nakamura et al., 2013). Pink line marks the decollement surface and blue arrow indicates the zone of topographic slope-break in both (b) and (c). (For interpretation of the references to colour in this figure legend, the reader is referred to the web version of this article.)

Table 1
Modeling parameters and material properties.

Parameter and model properties	Sand (analog model)	Natural prototypes	Ratio: model/nature
Length, L (m)	0.01	360	$\lambda = 2.7 \times 10^{-5}$
Density (kg m^{-3})	1600	2700	$\delta = 0.59$
Internal friction angle, ϕ (°)	~30	30–40	1–0.75
Cohesion (Pa)	20	2×10^6	1×10^{-5}
Gravity, g (m s^{-2})	9.8	9.8	$\gamma_g = 1$
Deviatoric stress[a]			
($\sigma = \delta$ g L)	157 Pa	9.5×10^6 Pa	16.5×10^{-6}
Velocity	5 mm/min	85 mm/yr	3.09×10^4

[a] Based on Schellart (2000).

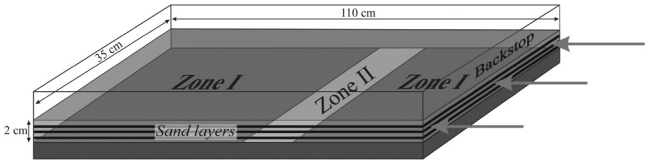

Fig. 2. A sketch of the experimental setup showing 3D view of the model setup. Zones I and II represent low and high frictional contact zone respectively. Arrows on the right show the direction of shortening.

We used dry, non-cohesive natural quartz-rich (>90%) well-rounded sand (average sphericity of 0.8), as analog material for scaled model experiments simulating crustal scale brittle deformation (Davis et al., 1983; Mulugeta, 1988; Koyi, 1995; Mandal et al., 1997; Schellart, 2000). The sand had a bulk density of 1600 kg/m^3, and a coefficient of internal friction close to 0.57. Our model scales to nature with a ratio of 2.7×10^{-5}, where 1 cm in the model is equivalent to 360 m in nature (Table 1). The cohesion of the model material (dry quartz sand) in our experiment is around 20 Pa, which scales to 2 MPa (Gutscher et al., 1998) for unconsolidated marine sediments (Hoshino et al., 1972). The models were deformed in a pure shear box at a uniform velocity of 5 mm/min using a computer controlled step-up motor by setting a backstop at the rear of the sand layers. Previous studies revealed that buttress geometry is important in the development of wedge geometry in sand layers (Byrne et al., 1998; Persson and Sokoutis, 2002). However, we used planar vertical buttress in our experimental setup in order to model a mono-vergent accretionary wedge as observed in the Japan Trench (Mulugeta, 1988; Storti and McClay, 1995; Gutscher et al., 1998; Bose et al., 2009). We have carried out two sets of experiments with different initial thickness of sand layers. According to

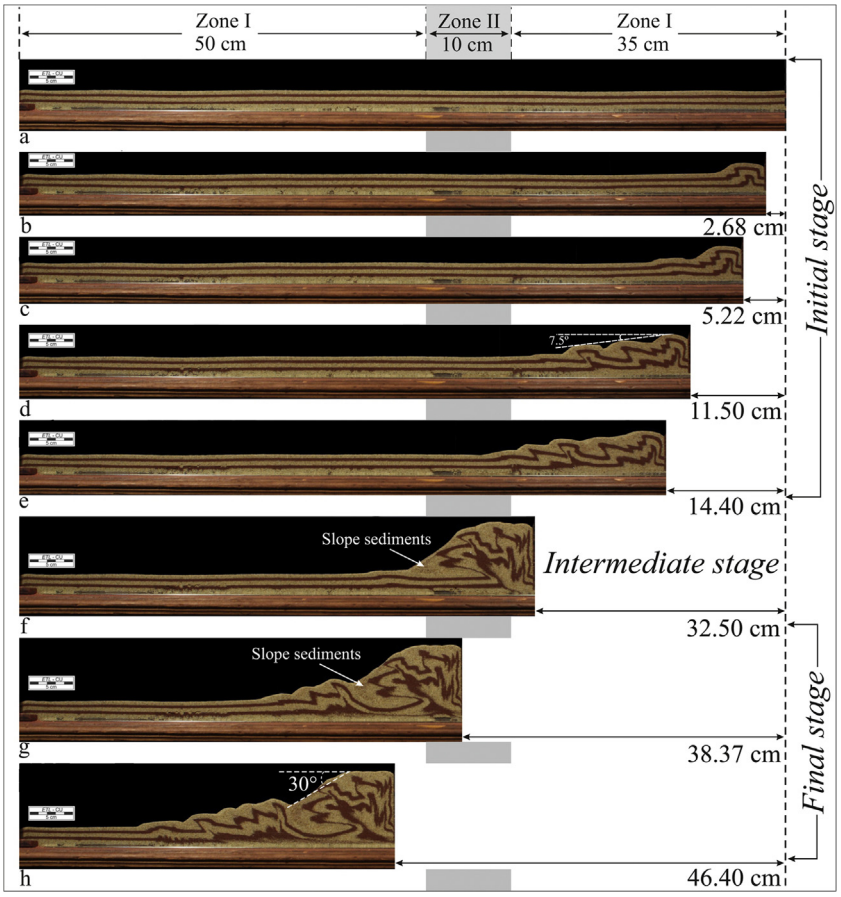

Fig. 3. Progressive development of frontal wedge in sand models with 10 cm width of Zone II. (a) Initial model, (b–e) initial stage, (f) intermediate stage and (g–h) progressive development of wedge during the final stage (see text for details). Note that the frontalward deformation propagation stopped after shortening of 14. 40 cm, but hinterland elevation continued to increase (e). 18.10 cm shortening was accommodated within the wedge, reorienting earlier structures during intermediate stage (f). Further shortening moves the deformation front above the lower frictional base developing a distinct slope-break (g–h).

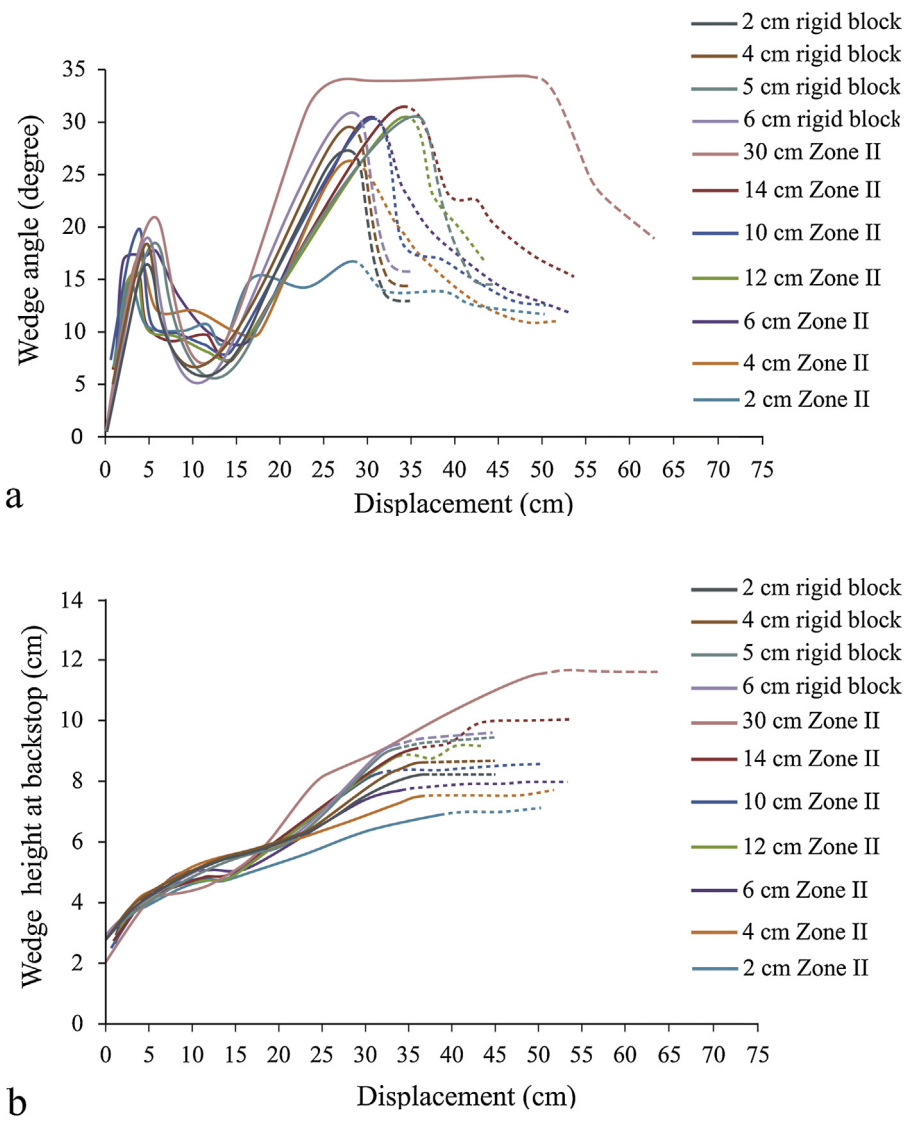

Fig. 4. Plots show different stages of wedge growth for varying width of zone II using high frictional patches (7 experiments) and rigid blocks (4 experiments). Wedge angle (a) and Wedge height at the backstop (b), are plotted as a function of actual displacement (horizontal shortening) in cm. In the initial stage of the wedge growth, wedge angle (a) and wedge height (b) reached a constant value with horizontal displacement. The intermediate stage marks the sharp increase in both wedge angle (solid line) (a) and wedge height (solid line) (b). In the final stage wedge height attained a constant value (dash line) (b) with decreasing wedge slope (dash line) (a).

our results this thickness does not significantly affect the development of first order geometry of the wedge (Fig. 3 and see electronic supplementary Fig. S2). Although a sand layer of 1 cm thickness would be ideal according to our scaling, we chose to present the results from the models with the 2 cm thickness because they better reproduce brittle structures within the wedge. During the experimental run, we photographed through the lateral glass wall after an interval of every 5 s, keeping the camera at a fixed distance from the model. Model deformations were analyzed from successive photographs taken during the experimental run.

3. Experimental results

In our experiments, the wedge started to grow above Zone I by in-sequence thrusting at the *initial stage* and developed a gentle surface slope (α) at uniform shortening rate (Figs. 3b and c, 4a). The height of the wedge at the backstop attained an almost stationary value when the model was shortened by 5 cm in all experiments (Fig. 4b). At this stage, the frontal propagation of the wedge dominated over the vertical growth through sequential thrusting until the deformation front reached Zone II. During this stage the wedge developed a critical taper, $\alpha = 7.5^\circ$ (Figs. 3d, 4a), which is closer to the theoretical value of surface slope (α) of 6° obtained from "equation 1" for $\beta = 0$, $\mu_b = 0.36$ and $\phi_c = 0.57$.

The mode of internal deformation and the wedge geometry changed completely when the deformation front reached the edge of the high frictional patch (Zone II, $\mu_b = 0.42$), simulating a horst (Fig. 3e, see electronic supplementary Figs. S1 A [d] and B [d]). At this stage, decollement propagation ceased and the established wedge formed over Zone I started deforming internally, increasing the wedge height consistently, and developing a steep topographic slope (Fig. 4). This stage of wedge growth has been defined as the *intermediate stage* (Fig. 3e and f). The topographic slope of the wedge at this stage became much higher than the predicted value (Eq. (1)), and the wedge grew to a super critical state. The cessation of decollement propagation promoted the development of supercritical wedge in order to accommodate the amount of horizontal shortening, and eventually facilitated slope failure (Fig. 3f). During this stage, we observed mechanical rotation and reorientation of already deformed sand layers in the hanging wall, giving rise to a complex deformation structures within the deforming wedge.

With further horizontal shortening, the deformation front crossed the Zone II and propagated onto the region above Zone I over low μ_b, simulating another graben of the deformation front advanced by in-sequence thrusting and eventually, developed a separate wedge with a low taper angle as predicted for low basal friction. These spatial and temporal variations in the style and intensity of deformation across the wedge finally gave rise to a distinct topographic slope-break in the wedge geometry separating the steep inner wedge from the low tapered outer wedge (Figs. 3g–h and 4a). During the growth of the outer wedge, the internal deformation in the inner wedge completely stopped (Fig. 4b) and the horizontal shortening was entirely accommodated by in-sequence thrusting over weak fictional base (Zone I). We describe this stage of wedge growth as the *final stage*, which is characterized by the development of a topographic slope-break with the cessation of internal deformation within the inner wedge. Experiments with varying width of Zone II showed that increasing the width of the Zone II (e.g. 30 cm) required large amount of shortening for the development of the topographic slope-break (Figs. 4 and 5, see electronic supplementary Fig. S3). The development of slope-break in the wedge geometry thus can be carefully used as a potential indicator for interpreting long-term frictional condition on the decollement.

Experiments with more than one high frictional patch (Zone II) on the basal fault showed that the surface slope of outer wedge (i.e., the wedge over low μ_b) started to deform again once the decollement propagation was resisted by another high frictional patch in the front. As a consequence, the surface slope of the outer wedge was completely modified along with the destruction of topographic slope-break (Fig. 6h). With further shortening the outer wedge progressively merged with the inner wedge, giving rise to a single wedge with steep uniform surface slope (Fig. 6i). During this process of wedge modification, the inactive inner wedge again resumed to deform by mechanically rotating all preexisting structures and thereby, increasing the complexity of deformation structures toward the hinterland part of the wedge (Fig. 6i and k). With continuous shortening, the deformation within this steep wedge completely stopped once the deformation front propagated over another low frictional base in the front with the onset of the development of new outer wedge by in-sequence thrusting (Fig. 6j and k). Based on above results, it is evident that the geometry of the frontal wedge is essentially transient with varying down-dip frictional strength on the decollement in tectonically active convergent belts over long time scale.

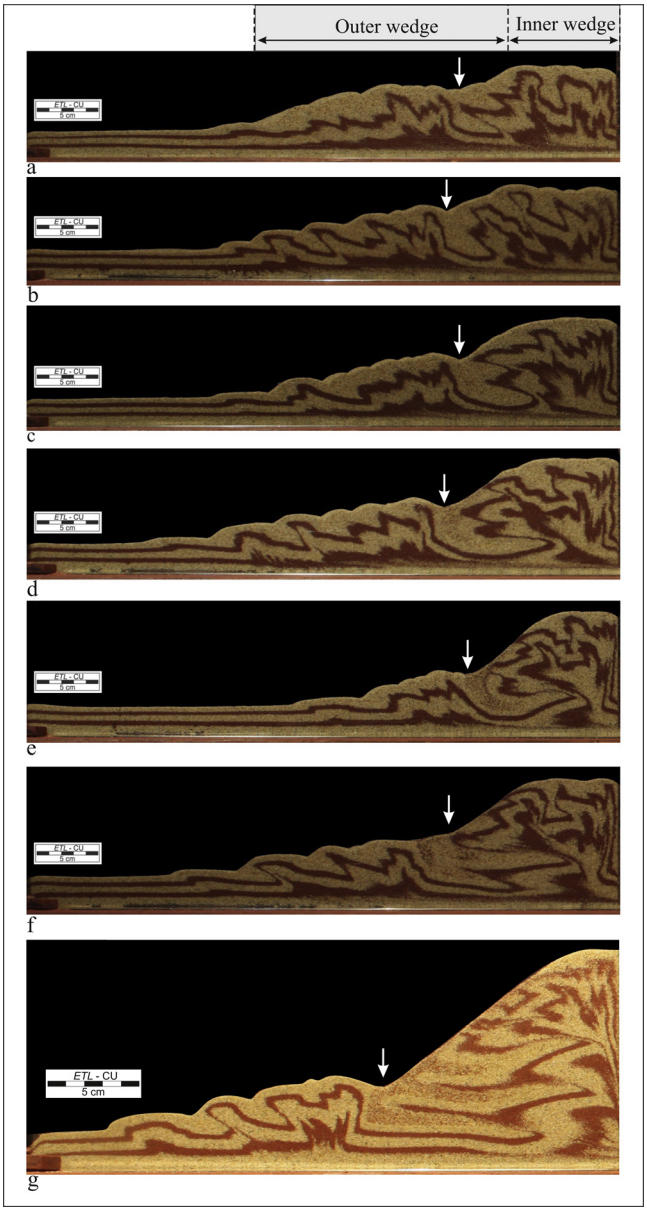

Fig. 5. Final stage of wedge development for varying widths of the high frictional patch: 2 cm (a), 4 cm (b), 6 cm (c), 10 cm (d), 12 cm (e), 14 cm (f) and 30 cm (g). The width of the model is 35 cm for all experiments. White arrow marks the zone of topographic slope-break between the inner and outer wedge.

4. Discussion

4.1. Consequence of down-dip variations in basal friction

On the basis of the above observations and interpretations on the experimental results we discuss below the role of basal friction in the structural development of frontal wedge near the Japan Trench. Our study reveals that varying down-dip frictional strength on the decollement causes a drastic change in the wedge taper, giving rise to a steep *inner wedge* and gentle *outer wedge*. This lateral change in the surface slope across the wedge separates the entire wedge into two distinctive structural domains: (i) complex internal deformation within *the inner wedge* and (ii) the *outer wedge* is deformed mostly by sequential thrusting. Experimental results show that the growth of the inner wedge begins by in-sequence thrusting over low frictional base following the model of critical angle of taper (Davis et al., 1983; Mulugeta, 1988; Koyi, 1995; Gutscher et al., 1998; Yamada et al., 2006; Bose et al., 2009). However, with ongoing shortening the taper angle of the wedge progressively steepens with the termination of decollement propagation by the increased frictional resistance along the decollement. The steepening of the wedge slope and intense internal deformation within it continues until the deformation front crosses from the zone of high to low friction on the basal decollement. The propagation of the deformation front onto the lower frictional base immediately stops internal deformation within the rear part of the wedge (Fig. 3g–h). The deformation front propagates by a new phase of in-sequence thrusting with continuing horizontal shortening, forming the shallow taper outer wedge. This process of wedge propagation over varying patches of basal friction thus gives rise to the development of topographic slope-break between the inner and the outer wedges. Our experimental results suggest that the topographic slope-break in the tectonic wedge becomes prominent when the lateral propagation of the deformation front over low frictional patch is significantly large (Fig. 5a–g).

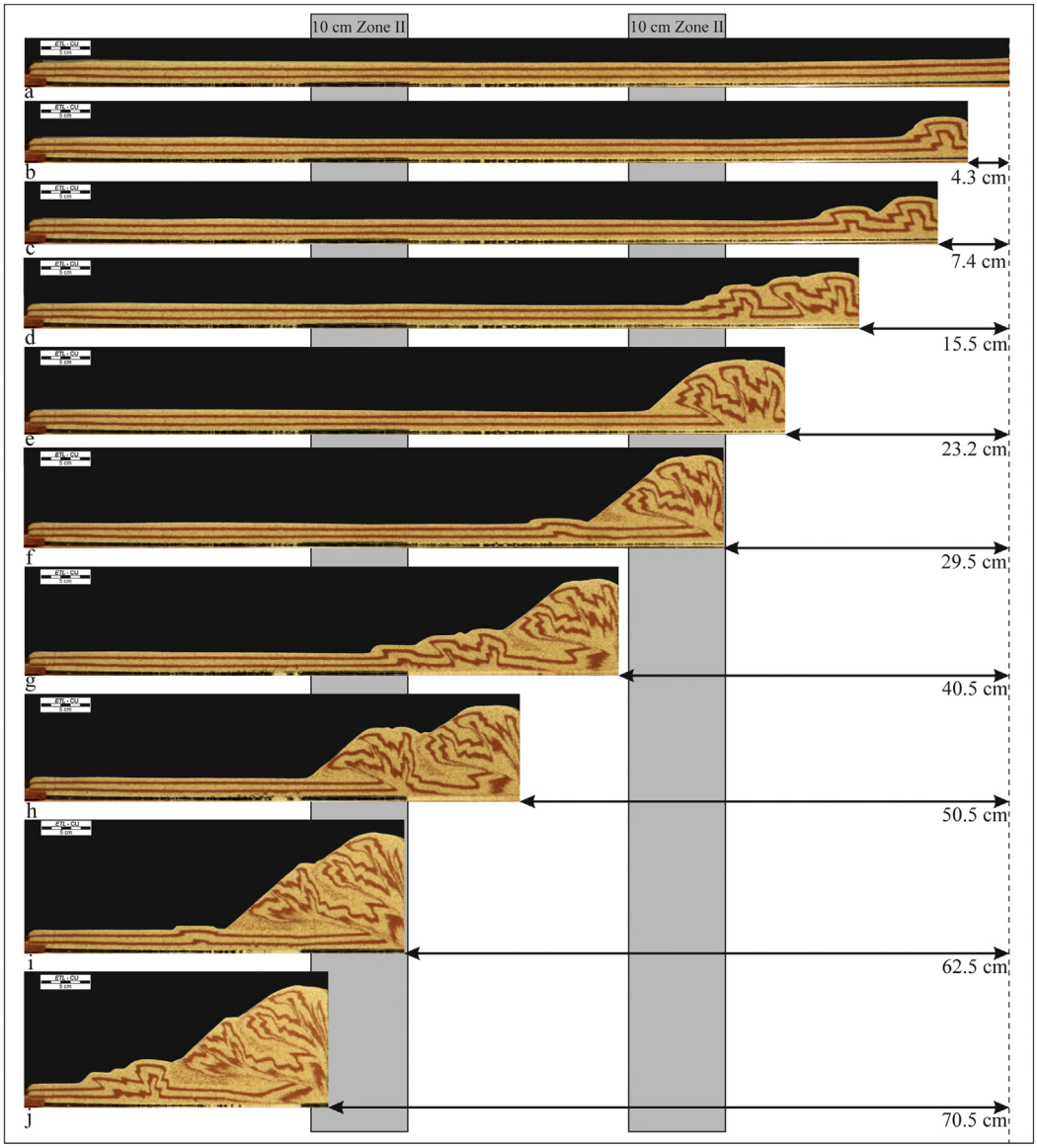

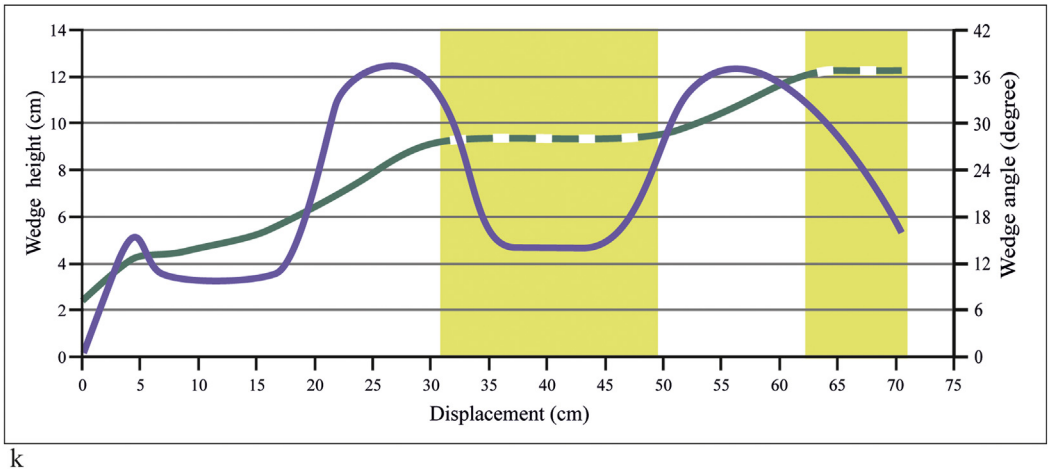

k

Fig. 6. Progressive development of frontal wedge growth over multiple high frictional patches, forming alternate uniform slope and topographic slope-break. (a–d) Initial stage, (e) intermediate stage with steep uniform slope, (f–g) final stage showing the development of a slope-break, (h) process of destruction of the outer wedge observed in figure (g) due to another high frictional patch in the front, leading to a steep uniform surface slope (i), (j) development of a new slope-break in the wedge geometry with low basal friction, (k) Plots show the variations of wedge angle (purple) and wedge elevation at the hinterland buttress (green) as a function of horizontal displacement. Note that the combination of low tapered wedge and constant wedge elevation implies growing of wedge over a low frictional base (yellow shade). (For interpretation of the references to colour in this figure legend, the reader is referred to the web version of this article.)

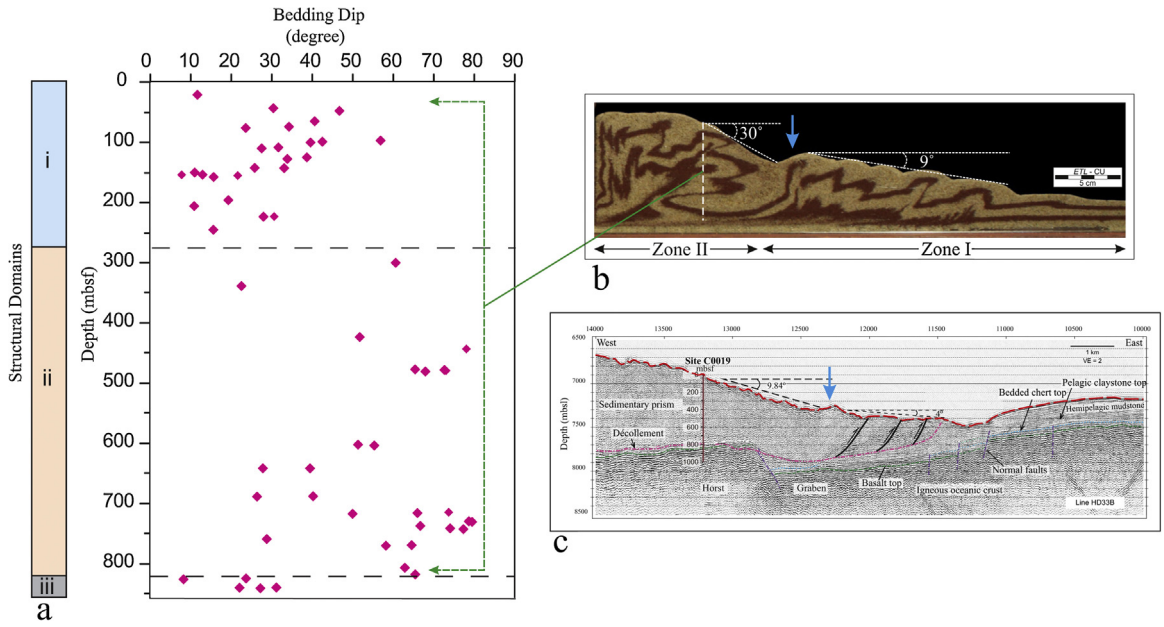

Fig. 7. Compilation of core data with depth at IODP site C0019 and comparison with experimental model. (a) Deformation unit in the core data shows variations in bedding dip with depth and three structural domains are identified. (i) Upper frontal prism (0–275 mbsf) shows gently inclined bedding, (ii) lower frontal prism (276–820 mbsf) showing variable and steeply dipping beds characterized by folded and faulted sediments, (iii) base section (820 mbsf to base of the hole) with shallow to horizontal bedding represents in the footwall block in the subduction zone (modified after Chester et al., 2013). (b) Experimental model shows resemblance in the changes of bedding orientations with depth. Green arrows show the region in the experimental model comparable with core data set. White dash line in the model replicates the drilling site C0019 shown in Fig. 7c. (c) Details and interpretations of seismic image along section HD 33B. Vertical exaggeration = 2:1 (Modified after Kodaira et al., 2012). Note that experimental model closely reproduces geometrical and structural features observed in seismic image. Both experimental and seismic sections show that the surface slope of the inner wedge is steeper than that of the outer wedge. Imbricate thrusts are prominent within the outer wedge. The blue arrow marks the zone of topographic slope-break between inner and outer wedges in Fig. 7b and c. (For interpretation of the references to colour in this figure legend, the reader is referred to the web version of this article.)

4.2. *Interpretation of wedge development near the Japan Trench*

The present study has an important implication for understanding the development of frontal wedge near the Japan Trench. Seismic sections across the Japan Trench show the change in slope of the frontal prism over subducting horst-and-graben structure from 10° in the landward part to 4° toward the trench (Fig. 1b). Comparing our experimental results with seismic data from frontal wedge near the Japan Trench suggests that down-dip variations in frictional strength along the basal decollement could have caused the present geometry of the wedge and deformation structures within it near the Japan Trench (Fig. 1b and c). Our experimental results suggest that the subduction of horst-and-graben structure into the Japan Trench could create varying degree of coupling across the decollement that eventually resulted in the development of the characteristic topographic slope-break. It further reveals that the steep slope over the horst block must have formed prior to the propagation of deformation front over the graben sediments. Our experimental study shows that initiation of growth of the outer wedge over low basal friction deactivates the internal deformation of the inner wedge. This has led to infer that the present day plate convergence near the Japan Trench is accommodating entirely by in-sequence thrusting in the graben sediments over low friction. Previous experimental findings (Huiqi et al., 1992; Bose et al., 2009) along with the present study indicate that the occurence of a series of imbricate thrusts over graben sediments, preserved in the outer wedge of the Japan Trench (Kodaira et al., 2012; Nakamura et al., 2013), have formed over relatively weak decollement (Fig. 7c).

The structural interpretations from the drill core samples collected during JFAST (Chester et al., 2013) and interpreted seismic profiles (Nakamura et al., 2013) reveal that the frontal prism over the subducted horst block (i.e., high frictional patch) is structurally chaotic, consistent with the observed deformation structures in our experimental models. The dip of beds measured in the core samples varies from 20° to 80° and they are also traversed by numerous closely spaced faults (Chester et al., 2013; Nakamura et al., 2013; Kirkpatrick et al., 2014) (Fig. 7). Our experimental results show that the complexity in the internal deformation within the inner wedge increases with the onset of steepening of the inner wedge slope when the frontal propagation of the decollement is resisted by the high frictional patch during ongoing shortening (Figs. 3 and 4). This suggests that the variably steeply dipping beds in the core samples might have evolved through the process of mechanical rotation of earlier structures within the hanging wall when the decollement propagation was either temporarily stopped or was very slow due to high-frictional resistance along the horst block. Based on the above discussions, it appears that subduction of horst-and-graben structure played a crucial role in increasing the complexity of deformation structures observed at the drill site near the Japan Trench. With continued plate convergence over time the deformation front eventually crossed the high frictional patch resulting in the break in the surface slope observed between the inner and outer wedges in the frontal prism. In the laboratory experiments, the break in the surface slope of the wedge becomes prominent once the backstop overrides the high frictional patch and consequently, develops an outer wedge by in-sequence thrusting (Figs. 3g, 6f and j). Comparing our experimental results with seismic images confirms that the buttress (~backstop in the experimental setup) in the Japan Trench forearc currently lies west of the JFAST drilling site toward landward part of the wedge, as predicted by earlier workers (Tsuru et al., 2002) (Fig. 7b and c). Our experimental results further reveal that the observed slope sediments between the inner and outer wedge in the Japan Trench might have accumulated during the growth of supercritical wedge as identified in the *intermediate stage* in experiments and the sediment accumulation continued until the deformation front crossed the horst block (Fig. 3f). This, however,

does not rule out the possibility of rotational slumping of the slope sediments in the frontal wedge by later reactivation during the 2011 megaearthquake event (Strasser et al., 2011).

Our experimental results also explain the lack of natural examples of the accretionary prisms displaying multiple slope-breaks. Experiments with two high frictional patches on the decollement show that the cessation of the propagation of outer wedge when encountering a high frictional patch modifies the wedge geometry thoroughly by mechanical rotation of all pre-existing deformation structures, forming a wedge with a uniformly steep surface slope (Fig. 6). These observations have led us to infer that the subduction of the horst block in the Pacific plate lying currently on the east of the Japan Trench will eventually modify the present wedge geometry from a distinct topographic slope-break to a uniformly steep slope.

5. Conclusion

Our main conclusions are as follows:

1) Down-dip frictional variations on the decollement cause temporal and spatial variations in the geometry of the frontal wedge.
2) Surface slope-break develops when the deformation front crosses from high to low basal friction. The break in the surface slope separates the entire wedge into two distinct structural domains: inner and outer wedges.
3) The inner wedge is characterized by a steep wedge slope and complex internal structures, whereas the outer wedge is deformed by in-sequence thrusting, leading to a shallow taper angle.
4) The experimental models explain well the structural evolution of the frontal wedge near the Japan Trench observed in seismic images and borehole data.
5) We interpret that the complexity of internal deformation observed in core samples and localization of the steep surface slope toward the landward part of the wedge near the Japan Trench is caused by the cessation of decollement propagation by the horst block in the subducting plate lying beneath the JFAST drill site.
6) The development of a shallow taper outer wedge over the graben sediments by in-sequence thrusting marks the cessation of internal deformation in the rear part of the wedge (i.e., inner wedge), creating the topographic slope-break near the Japan Trench.

Acknowledgements

We thank scientific and drilling staff on Drilling Vessel *Chikyu* for their constant assistance during the IODP expedition 343. We thank Ylona van Dinther and Marc-Andre Gutscher for their insightful reviews and constructive suggestions for improvement of this work. We also thank W.P. Schellart for his guidance in revising the manuscript. The work is supported by MOES, Govt. of India and DST, Govt. of India grants to SB and PS acknowledge CSIR, India for financial support.

AG acknowledges SRFP 2012 of Indian Science Academies.

Appendix A. Supplementary data

Supplementary data associated with this article can be found, in the online version, at http://dx.doi.org/10.1016/j.jog.2015.06.002

References

Bilek, S., 2007. Influence of subducting topography on earthquake rupture. In: Dixon, T., Moore, C. (Eds.), The Seismogenic Zone of Subduction Thrust Faults. Columbia University Press, p. 123.

Bose, S., Mandal, N., Mukhopadhyay, D.K., Mishra, P., 2009. An unstable kinematic state of the Himalayan tectonic wedge: evidence from experimental thrust-spacing patterns. J. Struct. Geol. 31, 83–91.

Boyer, S.E., Elliot, D., 1982. Thrust systems. Am. Assoc. Pet. Geol. 67, 1196–1230.

Byrne, D.E., Davis, D.M., Lynn, R.S., 1998. Loci and maximum size of thrust earthquakes and the mechanics of the shallow region of subduction zones. Tectonics 7, 833.

Chapple, W.M., 1978. Mechanics of thin-skinned fold-and-thrust belts. Geol. Soc. Am. Bull. 89, 1189.

Chester, F.M., Rowe, C., Ujiie, K., Kirkpatrick, J., Regalla, C., Remitti, F., Moore, J.C., Toy, V., Wolfson-Schwehr, M., Bose, S., Kameda, J., Mori, J.J., Brodsky, E.E., Eguchi, N., Toczko, S., 2013. Expedition 343 and 343T Scientists. Structure and composition of the plate-boundary slip zone for the 2011 Tohoku-Oki earthquake. Science 342, 1208–1211.

Dahlen, F.A., 1990. Critical taper model of fold-and-thrust belts and accretionary wedges. Annu. Rev. Earth Planet. Sci. 18, 55–99.

Das, S., Watts, A.B., 2009. Effects of subducting seafloor topography on the rupture characteristics of great subduction zone earthquakes. In: Lallemandand, S., Funiciello, F. (Eds.), Subduction Zone Geodynamics. Springer-Verlag, Berlin, Heidelberg, pp. 103–118.

Davis, D.M., Suppe, J., Dahlen, F.A., 1983. Mechanics of fold-and-thrust belts and accretionary wedges. J. Geophys. Res. 88, 1153–1172.

Dominguez, S., Malavieille, J., Lallemand, S.E., 2000. Deformation of accretionary wedges in response to seamount subduction: insights from sandbox experiments. Tectonics 19, 182–196.

Groshong, R.H., 2006. 3-D Structural Geology: A Practical Guide to Quantitative Surface and Surface Map Interpretation. Springer, New York, pp. 400.

Gutscher, M.A., Kukowski, N., Malavieille, J., Lallemand, S., 1998. Material transfer in accretionary wedges from analysis of a systematic series of analog experiments. J. Struct. Geol. 20 (4), 407–416.

Hoshino, K., Koide, H., Inmni, K., lwamuraa, S., Mitsui, S., 1972. Mechanical properties of Japanese teritary sedimentary rocks under high confining pressures. Geol. Surv. Jpn, Kawasaki, Japan, p200.

Huiqi, L., McClay, K.R., Powell, D., 1992. Physical models of thrust wedges. In: Thrust tectonics. Springer, Netherlands, pp. 71–81.

Kirkpatrick, J.D., Rowe, C.D., Ujiie, K., Moore, J.C., Regalla, C., Remitti, F., Toy, V., Wolfson-Schweh, M., Kameda, J., Bose, S., Chester, F.M., 2014. Structure and lithology of the Japan Trench subduction plate boundary fault. Tectonics 34, http://dx.doi.org/10.1002/2014TC003695

Kodaira, S., No, T., Nakamura, Y., Fujiwara, T., Kaiho, Y., Miura, S., Takahashi, N., Kaneda, Y., Taira, A., 2012. Coseismic fault rupture at the trench axis during the 2011 Tohoku-oki earthquake. Nat. Geosci. 5, http://dx.doi.org/10.1038/NGEO1547

Koyi, H., 1995. Mode of internal deformation of sand wedges. J. Struct. Geol. 17, 293–300.

Lallemand, S.E., Schnürle, P., Malavieille, J., 1994. Coulomb theory applied to accretionary and nonaccretionary wedges: possible causes for tectonic erosion and/or frontal accretion. J. Geophys. Res. 99, 12033–12055.

Lallemand, S.E., Malavieille, J., Calassou, S., 1992. Effects of oceanic ridge subduction on accretionary wedges: experimental modeling and marine observations. Tectonics 11 (6), 1301–1313.

Malavieille, J., 1984. Modelisation experimentale des chevauchements imbriques; application aux chaines de montagnes. Bull. Soc. Géol. Fr. (1), 129–138.

Mandal, N., Chattopadhyay, A., Bose, S., 1997. Imbricate thrust spacing: experimental and theoretical analyses. In: Sengupta, S. (Ed.), Evolution of Geological Structures in Micro- to Macro-Scales. Chapman and Hall, London, p. 143.

Mulugeta, G., 1988. Modeling the geometry of Coulomb thrust wedges. J. Struct. Geol. 10, 847.

Nakamura, Y., Kodaira, S., Miura, S., Regalla, C., Takahashi, N., 2013. High resolution seismic imaging in the Japan Trench axis area of Miyagi. Northeast. Jpn. Geophys. Res. Lett. 40, 1713–1718, http://dx.doi.org/10.1002/grl.50364

Pacheco, J.F., Sykes, L.R., Scholtz, C.H., 1993. Nature of seismic coupling along simple plateboundaries of the subduction type. J. Geophys. Res 98, 14133–14159.

Park, J.O., Tsuru, T., Kaneda, Y., Kono, Y., Kodaira, S., Takahashi, N., Kinoshita, H., 1999. A subducting seamount beneath the Nankai accretionary prism off Shikoku, southwestern Japan. Geophys. Res. Lett. 26 (7), 931–934.

Persson, K.S., Sokoutis, D., 2002. Analogue models of orogenic wedges controlled byerosion. Tectonophysics 356, 323.

Schellart, W.P., 2000. Shear test results for cohesion and friction coefficients for different granular materials: scaling implications for their usage in analogue modelling. Tectonophysics 324 (1), 1–16.

Souloumiac, P., Mailot, B., Leroy, Y.M., 2012. Bias due to side wall friction in sand box experiments. J. Struct. Geol. 35, 90–101.

Storti, F., McClay, K.R., 1995. Influence of syntectonic sedimentation thrust wedges in analogue models. Geology 23, 999.

Strasser, M., Kölling, M., dos Santos Ferreira, C., Fink, H.G., Fujiwara, T., Henkel, S., Ikehara, K., Kanamatsu, T., Kawamura, K., Kodaira, S., Römer, M., Wefer, G., 2011. The R/V Sonne Cruise SO219A and JAMSTEC Cruise MR12-E01 scientists, 2013. A slump in the trench: tracking the impact of the Tohoku-Oki earthquake. Geology 41, 935–938.

Tanioka, Y., Ruff, L., Satake, K., 1997. What controls the lateral variation of large earthquake occurrence along the Japan Trench? Island Arc. 6, 261–266.

Tsuru, T., Park, J.O., Miura, S., Kodaira, S., Kido, Y., Hayashi, T., 2002. Along-arc structural variation of the plate boundary at the Japan Trench margin: implication of interplate coupling. J. Geophys. Res. 107 (B12), 1–15, ESE-11.

von Huene, R., Culotta, R., 1989. Tectonic erosion at the front of the Japan Trench convergent margin. Tectonophysics 160, 75–90.

von Huene, R., Lallemand, S., 1990. Tectonic erosion along the Japan and Peru convergent margins. Geol. Soc. Am. Bull. 102, 704–720.

von Huene, R., Ranero, C.R., Vannucchi, P., 2004. Generic model of subduction erosion. Geology 32, 913–916.

von Huene, R., Klaeschen, D., Fruehn, J., 1999. Relation between the subducting plate and seismicity associated with the Great 1964 Alaska earthquake. Pure Appl. Geophys. 154, 575.

Wang, K., Hu, Y., 2006. Accretionary prisms in subduction earthquake cycles: the theory of dynamic Coulomb wedge. J. Geophys. Res. B06410, http://dx.doi.org/10.1029/2005JB004094

Yamada, Y., Baba, K., Matsuoka, T., 2006. Analogue and numerical modeling of accretionary prisms with a decollement in sediments. In: Buiter, S.J.H., Schreurs (Eds.), Analogue and Numerical Modeling of Crustal-scale Processes, 253. Geol. Soc. London Spec. Pub, pp. 169–183.